# NATIONAL ADVISORY COMMITTEE FOR AERONAUTICS

**TECHNICAL NOTE 3135** 

INVESTIGATION OF MUTUAL INTERFERENCE EFFECTS OF SEVERAL

VERTICAL-TAIL—FUSE LAGE CONFIGURATIONS IN SIDESLIP

By William H. Michael, Jr.

Langley Aeronautical Laboratory Langley Field, Va.



Washington
January 1954

#### NATIONAL ADVISORY COMMITTEE FOR AERONAUTICS

## TECHNICAL NOTE 3135

INVESTIGATION OF MUTUAL INTERFERENCE EFFECTS OF SEVERAL

VERTICAL-TAIL-FUSELAGE CONFIGURATIONS IN SIDESLIP

By William H. Michael, Jr.

#### SUMMARY

Tests were made on three circular-arc-fuselage and nine unsweptvertical-tail models in order to investigate interference effects between fuselages and vertical tails in sideslip. The mutual interference effects, and thus the effectiveness of the vertical tail in producing directional stability, appear to be mainly dependent upon the ratio of the vertical-tail span to the fuselage diameter at the position of the vertical tail and upon the vertical-tail aspect ratio and to be relatively independent of the fuselage fineness ratio. The increase in verticaltail effectiveness is largest for small values of the ratio of the vertical-tail span to the fuselage diameter and decreases as this ratio increases; in general, the effectiveness increases with increase in the vertical-tail aspect ratio. The magnitude of the induced loading on the fuselage is comparable to the magnitude of the corresponding induced loading on the vertical tail. The interference effects of the vertical tail and the fuselage on one another may result in a tail effectiveness of the tail-fuselage combination which is different from that of the tail alone, the difference being an increase of 0 to 100 percent of the tail-alone effectiveness for the configurations tested. The vertical center-of-pressure calculations indicate that, as the span-to-diameter ratio decreases, the fuselage loading becomes proportionally more important and the center of pressure moves downward toward the tail root or the fuselage center line. The longitudinal center of pressure is in the vicinity of the tail quarter-chord line.

Some theoretical calculations of the interference effect of a cylindrical body on adjacent lifting surfaces gave good agreement with the corresponding measured values for the vertical-tail plan forms considered.

#### INTRODUCTION

Analyses of present-day airplanes have indicated that interference effects between component parts of airplanes have a significant influence on aircraft loads and stability derivatives. This influence is found to

be important in the case of mutual interference between the fuselage and the vertical tail. A number of experimental investigations have been made to determine the effects of various fuselage, vertical-tail, and horizontal-tail combinations on complete-model characteristics (for instance, refs. 1 to 4). Little information is available, however, which gives an indication of the relative loading on the component parts or of the mutual interference between the parts, as affected by fuselage and vertical-tail geometric characteristics.

The purpose of the present investigation is to determine the mutual interference effects between the fuselage and the vertical tail by measuring the forces and moments on the model components separately and in combination and then finding the differences. The models used in the investigation consisted of fuselage and vertical-tail components only. Some theoretical calculations also were made to determine the interference effect of a cylindrical body on adjacent lifting surfaces and the results are compared with the experimental data.

#### SYMBOLS AND COEFFICIENTS

Positive directions of forces, moments, and angles are shown in figure 1. The symbols and coefficients used herein are defined as follows:

α	angle of attack, deg
A	aspect ratio
β	angle of sideslip, deg
bt	tail span, ft
$b_{\overline{W}}$	assumed wing span, ft
С	chord, ft
D	fuselage diameter, diameter of fuselage at position of vertical-tail quarter-chord line, ft
lt	tail length, horizontal distance from center of gravity of model to tail quarter-chord line, ft
lte bw	effective tail-length parameter, $\frac{b_{t}}{b_{w}} \frac{Cn_{\beta}}{CY_{\beta}}$
q	dynamic pressure, lb/sq ft

St vertical-tail area, sq ft

Sw assumed wing area, sq ft

z vertical distance, measured from intersection of vertical-tail quarter-chord line and fuselage surface, ft

L rolling moment, ft-lb

N yawing moment, ft-lb

Y lateral force, lb

 $c_l$  rolling-moment coefficient,  $\frac{L}{qS_tb_t}$ 

Cn yawing-moment coefficient, N/qStbt

 $C_{Y}$  lateral-force coefficient,  $\frac{Y}{qS_{t}}$ 

$$C_{l_{\beta}} = \frac{\partial C_{l}}{\partial \beta}$$

$$C_{n_{\beta}} = \frac{\partial C_{n}}{\partial \beta}$$

$$CA^{\beta} = \frac{9^{\beta}}{9^{CA}}$$

# Subscripts:

t isolated vertical-tail contribution

Δ<sub>1</sub> contribution due to interference effect of fuselage on vertical tail

contribution due to interference effect of vertical tail on fuselage

## APPARATUS AND TESTS

The models used in this investigation consisted of three mahogany circular-arc fuselages and nine mahogany vertical tails. Sketches of

the vertical tails and fuselages are given in figure 2 and geometric characteristics of the tails are given in table I. The vertical tails had zero sweep of the quarter-chord line, a taper ratio of 0.6, and NACA 65A008 profiles in sections perpendicular to the quarter-chord line. The three fuselages had circular cross sections and fineness ratios of 10.0, 6.67, and 5.0. The maximum thickness was the same for all three fuselages. The fuselages and vertical tails are designated as indicated in figure 2.

The vertical tails were attached to the fuselages through a straingage arrangement which allowed the lateral force and root bending moment of the tail to be measured independently of the measurements on the complete model (i.e., fuselage plus vertical tail). Figure 3 is a photograph of a vertical tail attached to a strain gage. Figure 4 is a photograph of a complete configuration mounted on the support strut. Each fuselage had one mounting position for the vertical tails such that the trailing edges of the tails with the largest chords extended to the trailing edge of the fuselage. Fuselage  $F_3$  had only one mounting position, but fuselages  $F_1$  and  $F_2$  each had two mounting positions, one as described and another at a more forward position at which the fuselage diameter was the same as the fuselage diameter at the mounting position on fuselage  $F_3$  (see fig. 2(b)).

Sideslip tests to determine the lateral force on the isolated vertical tails were made with an arrangement which was designed to give what was considered to be a minimum of interference from the supporting members. The strain gage was mounted on a metal bar which extended well forward of the support strut, and the vertical tails were connected to the gages by another bar attached to approximately the midspan of the vertical tail. The arrangement is shown in the photograph presented as figure 5.

Tests were made through a sideslip-angle range of  $\pm 10^{\circ}$  for the fuselages alone and for each vertical tail at all the fuselage positions, and balance-system measurements were made of the lateral force, rolling moment, and yawing moment. Although this investigation did not undertake a thorough study of the effects of angle of attack, results for both  $\alpha = 0^{\circ}$  and  $\alpha = 10^{\circ}$  are presented to give some indication of the effects of angle of attack.

All tests were made in the 6-foot-diameter rolling-flow test section of the Langley stability tunnel. The tests were made at a dynamic pressure of 40 pounds per square foot, corresponding to a Reynolds number range of  $3.90 \times 10^5$  to  $7.78 \times 10^5$  based on the average tail chord.

Jet-boundary corrections were not applied to the data because the corrections were found to be negligible. Also, no corrections were applied for effects of tunnel blockage or support-strut interference.

#### PRESENTATION OF RESULTS

The stability-derivative data obtained in this investigation, consisting of results obtained from the strain-gage measurements and the balance-system measurements, are presented in tables II and III. The derivatives were obtained from the slopes of faired curves drawn through the experimental-data plots of the forces and moments against the angle of sideslip. The slopes were taken at  $\beta=0^{\circ}$  and were in most cases linear through a range of sideslip angle of approximately  $\pm 8^{\circ}$ . In table II and in the discussion, the derivatives are based on the individual tail dimensions for convenience in making comparisons. For the balance-system results presented in table III, the derivatives were based on a constant assumed wing area of 2.25 square feet and a span of 3.0 feet in order to give an indication of the relative magnitude of the results obtained. The moment results from the strain-gage tests are not presented in table II but are used in the discussion to determine the vertical location of the centers of pressure.

#### DISCUSSION OF RESULTS

### Effectiveness of Isolated Vertical Tails

The results of the measurements of  $(C_{Y_{\beta}})_t$  are presented in figure 6 as a function of the vertical-tail aspect ratio. The small amount of scatter noted in cases where results for three tails of the same aspect ratio are presented is considered to be within the experimental accuracy of the results, when the large differences in tail areas are considered. Although the differences between the results for  $\alpha = 0^\circ$  and  $\alpha = 10^\circ$  are approximately of the same order as the scatter for a given aspect ratio, the results for  $\alpha = 10^\circ$  are generally somewhat higher than those for  $\alpha = 0^\circ$ , possibly because of the effects of the blunt root section. Values of  $(C_{Y_\beta})_t$  estimated in reference 5 (for  $\alpha = 0^\circ$ ) and calculated by the use of a simple vortex system consisting of six horseshoe vortices distributed over the vertical-tail span are included in figure 6 for the purposes of comparison.

In subsequent parts of the paper where the isolated vertical-tail results are used as a basis for obtaining ratios of interference effects, the measured isolated vertical-tail results for  $\alpha=0^{\circ}$  are used exclusively.

# Effectiveness of Vertical Tail Plus Mutual Interference of

## Fuselage and Vertical Tail

The force-test results for the complete model (fuselage plus vertical tail) minus the results for the fuselage alone were used to obtain  $({}^{\text{CY}}_{\beta})_{t+\Delta_1+\Delta_2}$ , which is plotted in figure 7 as a function of the ratio of the vertical-tail span to the fuselage diameter  $\frac{b_t}{D}$ , which was shown in references 2 and 5 to be an important parameter. The fuselage diameter is taken as the diameter of the fuselage at the location of the quarter-chord line of the vertical tail. The derivatives are based on the individual tail areas.

Faired curves were drawn through the data in figure 7 for each vertical-tail aspect ratio considered; the curves show that the magnitude of  $(C_{Y_{\beta}})_{t+\Delta_1+\Delta_2}$  increases with increasing aspect ratio and decreases as the ratio of tail span to fuselage diameter increases. For the cases in which a given vertical tail is mounted at a constant fuselage diameter (constant  $\frac{b_t}{D}$ ) on each of the three fuselages, the points are well grouped and show little variation with fuselage fineness ratio. Figure 8 shows the variation of  $(C_{Y_{\beta}})_{t+\Delta_1+\Delta_2}$  with fuselage length for the  $\alpha=0^{\circ}$  points presented in figure 7 which have constant values of  $\frac{b_t}{D}$ . The variations with fuselage length show no consistent trends, a condition which is typical of the results at  $\alpha=10^{\circ}$  also, and the variations are relatively small. Thus, the fuselage length and the longitudinal position of the vertical tail on the fuselage appear to be secondary parameters in influencing the vertical-tail effectiveness and the fuselage and vertical-tail interference effects.

The results presented in figure 7 for  $\alpha=0^{\circ}$  and  $\alpha=10^{\circ}$  are very similar, with the exception that, for the vertical tails of higher aspect ratio, the results for  $\alpha=10^{\circ}$  are slightly smaller in magnitude in the low range of  $\frac{b_t}{D}$  than those for  $\alpha=0^{\circ}$ .

The magnitude of the combined mutual interference effects of the fuselage—vertical-tail combination  $({}^{\text{C}}{}_{\gamma})_{\Delta_1+\Delta_2}$  can be found by subtracting  $({}^{\text{C}}{}_{\gamma})_{t}$  (presented in table II and discussed in the preceding section) from the results of figure 7. The combined interference effects may be a significant part of the total tail effectiveness, ranging from about 0 to 100 percent of the tail-alone effectiveness, the interference effects increasing as the tail aspect ratio increases and as the ratio of tail span to fuselage diameter decreases.

# Interference of Fuselage on Vertical Tail

The results of the strain-gage measurements of  $({}^{C}Y_{\beta})_{t+\Delta_{1}}$  are shown in figure 9. The results are presented with  $({}^{C}Y_{\beta})_{t+\Delta_{1}}$  as a function of the ratio of tail span to fuselage diameter  $\frac{b_{t}}{D}$ . Faired curves were drawn through the data and show that the magnitude of  $({}^{C}Y_{\beta})_{t+\Delta_{1}}$  more nearly

approximates the isolated vertical-tail values for each aspect ratio as  $\frac{b_t}{D}$  increases. The values for  $\alpha = 10^\circ$  are slightly smaller than those for  $\alpha = 0^\circ$  in the low range of  $\frac{b_t}{D}$ , a difference which indicates that in this range the vertical-tail—fuselage combination decreases slightly in effectiveness as the angle of attack increases.

The differences between the faired curves of  $(C_{Y_{\beta}})_{t+\Delta_1}$  (fig. 9) and the results for the isolated vertical tails (fig. 6) gave the interference effects of the fuselage on the vertical tail  $(C_{Y_{\beta}})_{\Delta_1}$ . The values of  $(C_{Y_{\beta}})_{\Delta_1}$  for the range of vertical-tail aspect ratios considered are presented in figure 10(a) for  $\alpha = 0^{\circ}$  and  $\alpha = 10^{\circ}$ . The values of  $(C_{Y_{\beta}})_{\Delta_1}$  show the previously observed trend of an increase in magnitude with increase in aspect ratio and a decrease in magnitude with increase in the ratio of span to diameter. The values for  $\alpha = 10^{\circ}$  are somewhat smaller in magnitude than those for  $\alpha = 0^{\circ}$ .

In order to compare the magnitude of  $({}^{C}Y_{\beta})_{\Delta_1}$  with the magnitude of the isolated vertical-tail results, plots of  $\frac{({}^{C}Y_{\beta})_{\Delta_1}}{({}^{C}Y_{\beta})_{t}}$  are presented in figure 10(b). As can be seen, the interference effects result in an increase in  $({}^{C}Y_{\beta})_{t}$  which may constitute a large part of the isolated vertical-tail effectiveness, depending on the vertical-tail aspect ratio and  $\frac{b_t}{D}$ . The ratio of  $({}^{C}Y_{\beta})_{\Delta_1}$  to  $({}^{C}Y_{\beta})_{t}$  is shown to decrease for the tail of aspect ratio 4.0, a result which indicates that there is probably an aspect ratio between 2.81 and 4.0 for which the magnitude of the fuselage interference is a maximum.

## Interference of Vertical Tail on Fuselage

The difference between the measurements of  $(CY_\beta)_{t+\Delta_1+\Delta_2}$  and  $(CY_\beta)_{t+\Delta_1}$  was used to obtain measurements of the interference of the vertical tail on the fuselage  $(CY_\beta)_{\Delta_2}$ . The values of  $(CY_\beta)_{\Delta_2}$  for the range of aspect ratio considered are presented in figure ll(a). The results for  $\alpha=0^\circ$  show a trend of increasing effectiveness with increasing aspect ratio and decreasing  $\frac{b_t}{D}$ , except that the results for the tail of aspect ratio 4.0 fall below the results for some of the tails of lower aspect ratio. The results for  $\alpha=10^\circ$  show this same trend of increasing interference effect with increasing aspect ratio. The magnitudes of the interference effects are somewhat similar for large values of the span-to-diameter ratio for all aspect ratios and for both angles of attack.

A significant result to be noted from these figures is that the interference of the vertical tail on the fuselage is comparable in magnitude to the fuselage interference on the tail, a condition which indicates that the induced loading carried by the fuselage in a vertical-tail—fuselage combination is an important consideration. The induced loading on the fuselage can apparently be as large as, or larger than, the induced loading on the vertical tail.

In order to compare the magnitude of the vertical-tail interference on the fuselage with the magnitude of the isolated vertical-tail effectiveness, the ratio of  $\begin{pmatrix} C_{Y_{\beta}} \end{pmatrix}_{\Delta_2}$  to  $\begin{pmatrix} C_{Y_{\beta}} \end{pmatrix}_{t}$  is plotted in figure ll(b). For  $\alpha = 0^{\circ}$ , the magnitude of the ratio of  $\begin{pmatrix} C_{Y_{\beta}} \end{pmatrix}_{\Delta_2}$  to  $\begin{pmatrix} C_{Y_{\beta}} \end{pmatrix}_{t}$  increases with vertical-tail aspect ratio until at some aspect ratio between 2.81 and 4.0 it reaches a maximum value for each  $\frac{b_t}{D}$ . A comparison of figure l0(b) and figure ll(b) illustrates that  $\frac{\begin{pmatrix} C_{Y_{\beta}} \end{pmatrix}_{\Delta_2}}{\begin{pmatrix} C_{Y_{\beta}} \end{pmatrix}_{t}}$  is, in general, comparable in magnitude to  $\frac{\begin{pmatrix} C_{Y_{\beta}} \end{pmatrix}_{\Delta_1}}{\begin{pmatrix} C_{Y_{\beta}} \end{pmatrix}_{t}}$  for comparable values of vertical-tail aspect ratio and ratio of tail span to fuselage diameter.

C

# Longitudinal Position of Center of Pressure

## of Combined Loading

In figure 12 are shown plots of effective tail lengths  $\frac{l_t}{b_W}$  and geometric tail lengths  $\frac{l_t}{b_W}$  for  $\alpha=0^\circ$  and  $\alpha=10^\circ$ . In order to find  $\frac{l_t}{b_W}$  for  $\alpha=10^\circ$ , the tail vertical center-of-pressure location was assumed to be at the tail semispan  $\frac{b_t}{2}$  along the quarter-chord line. Figure 12 shows that, except for some of the tails with small values of  $\frac{b_t}{D}$  and relatively long tail lengths, the effective tail lengths are nearly equal to the horizontal distances from the center of gravity to the tail quarter-chord line. Thus, in general, the combined loading  $(Cy_\beta)_{t+\Delta_1+\Delta_2}$  appears to be centered in the vicinity of the vertical-tail quarter-chord line. In particular, these results indicate that the induced loading on the fuselage  $(Cy_\beta)_{\Delta_2}$  is probably centered in the vicinity of the vertical-tail quarter-chord line.

## Vertical Location of the Center of Pressure

Vertical-tail loading. The strain-gage measurements of the forces and moments on the vertical tails were used to find the center of pressure of the vertical-tail loading  $({}^{C}Y_{\beta})_{t+\Delta_1}$ . The results are plotted in figure 13 as vertical center-of-pressure position above the vertical-tail root, for  $\alpha=0^{\circ}$  and  $\alpha=10^{\circ}$ . For the tails with large values of  $\frac{b_t}{D}$  the center of pressure is at approximately 45 percent of the tail span above the tail root for both  $\alpha=0^{\circ}$  and  $\alpha=10^{\circ}$ , and the center of pressure moves downward as  $\frac{b_t}{D}$  decreases, a result which indicates that a large part of the load is carried in the vicinity of the tail root on the tails with low values of  $\frac{b_t}{D}$ .

Combined loading. The vertical center-of-pressure locations for the combined loading  $({}^{\text{C}}\!Y_\beta)_{t+\Delta_1+\Delta_2}$  are plotted in figure 14, again in percent tail span above or below the vertical-tail root. A curve which represents the fuselage center line is included. A comparison of the data presented in figures 13 and 14 indicates that the induced effects of the vertical

tail on the fuselage cause the combined loading  $({}^{C}Y_{\beta})_{t+\Delta_1+\Delta_2}$  to be centered nearer the fuselage center line than was the vertical-tail loading  $({}^{C}Y_{\beta})_{t+\Delta_1}$ . The center of pressure for the combined loading for the tails with large values of  $\frac{b_t}{D}$  is about 30 to 35 percent of the tail span above the tail root; whereas for tails with smaller values of  $\frac{b_t}{D}$  the loading is centered nearer the fuselage. For the tails with the smallest values of  $\frac{b_t}{D}$  the loading is centered on the top half of the fuselage itself. Thus, for the tails with large values of  $\frac{b_t}{D}$ , the fuselage loading  $({}^{C}Y_{\beta})_{\Delta 2}$  is a small percentage of the combined loading; whereas for the tails with small values of  $\frac{b_t}{D}$  the loading on the fuselage becomes an important part of the combined loading (see fig. 11), a condition which causes the center of pressure to be near the tail root or perhaps even below the tail root.

# Comparison With Some Theoretical Calculations

In view of the fact that the fuselage interference on the vertical tail appears to be only slightly dependent upon the fuselage fineness ratio, some calculations were made to determine the interference effects of infinitely long circular cylinders on adjacent lifting surfaces. The method used in the calculations is similar to that used in reference 6 for calculating wing-fuselage interference effects, except that in the present calculations no corrections are made for finite body length or for rigorously satisfying the fuselage boundary conditions. In the present calculations, the vertical tails are represented by a horseshoe vortex system with images situated inside the cylinder at the proper positions. The velocities induced at the three-quarter-chord points of the vertical tail by the vortex system and the image vortex system are set equal to the velocity distribution on the vertical tail due to sideslip angle and the influence of the fuse lage. Solution of the set of simultaneous equations gives the vortex strengths and thus the forces on the vertical tails.

The results of the calculations are presented in figure 15 along with the corresponding experimental results from figure 9. In general, these calculations appear to provide a good estimation of the increase in effectiveness of the vertical tail due to the presence of the fuselage for the configurations considered.

#### CONCLUSIONS

Tests made in sideslip on three circular-arc-fuselage and nine vertical-tail models to determine mutual interference effects between fuselages and vertical tails have resulted in the following conclusions:

- 1. The mutual interference effects, and thus the vertical-tail effectiveness in producing directional stability, appear to be mainly dependent upon the ratio of the vertical-tail span to the fuselage diameter at the position of the vertical tail and on the vertical-tail aspect ratio and to be relatively independent of fuselage fineness ratio.
- 2. The increase in vertical-tail effectiveness due to interference is largest for small values of the ratio of the vertical-tail span to the fuselage diameter and decreases as this ratio increases. The interference effect in general increases with increase in vertical-tail aspect ratio.
- 3. The magnitude of the induced loading on the fuselage is comparable to that of the corresponding induced loading on the vertical tail.
- 4. The interference effects of the vertical tail and the fuselage on one another may result in a tail effectiveness of the tail-fuselage combination which is different from that of the tail alone, the difference being an increase of 0 to 100 percent of the tail-alone effectiveness for the configurations tested.
- 5. The vertical center-of-pressure calculations indicate that as the ratio of the span to the diameter decreases, the fuselage loading becomes proportionally more important and the center of pressure moves downward toward the tail root or the fuselage center line. The longitudinal center of pressure is located in the vicinity of the tail quarter-chord line.
- 6. Some theoretical calculations of the interference effect of a cylindrical body on adjacent lifting surfaces gave good agreement with the corresponding measured values for the vertical-tail plan forms considered.

Langley Aeronautical Laboratory,
National Advisory Committee for Aeronautics,
Langley Field, Va., November 2, 1953.

#### REFERENCES

- 1. Pass, H. R.: Analysis of Wind-Tunnel Data on Directional Stability and Control. NACA TN 775, 1940.
- 2. Queijo, M. J., and Wolhart, Walter D.: Experimental Investigation of the Effect of Vertical-Tail Size and Length and of Fuselage Shape and Length on the Static Lateral Stability Characteristics of a Model With 45° Sweptback Wing and Tail Surfaces. NACA Rep. 1049, 1951. (Supersedes NACA TN 2168.)
- 3. Letko, William: Effect of Vertical-Tail Area and Length on the Yawing Stability Characteristics of a Model Having a 45° Sweptback Wing. NACA TN 2358, 1951.
- 4. Brewer, Jack D., and Lichtenstein, Jacob H.: Effect of Horizontal Tail on Low-Speed Static Lateral Stability Characteristics of a Model Having 45° Sweptback Wing and Tail Surfaces. NACA TN 2010, 1950.
- 5. Lyons, D. J., and Bisgood, P. L.: An Analysis of the Lift Slope of Aerofoils of Small Aspect Ratio, Including Fins, With Design Charts for Aerofoils and Control Surfaces. R. & M. No. 2308, British A.R.C., 1945.
- 6. Zlotnick, Martin, and Robinson, Samuel W., Jr.: A Simplified Mathematical Model for Calculating Aerodynamic Loading and Downwash for Wing-Fuselage Combinations With Wings of Arbitrary Plan Form. NACA TN 3057, 1954. (Supersedes NACA RM L52J27a.)

TABLE I

GEOMETRIC CHARACTERISTICS OF VERTICAL TAILS

Vertical tail	Span, in.	Aspect ratio	Area, sq in.	Root chord, in.	Taper ratio
$v_1$	16	2.0	128	10.0	0.6
v <sub>2</sub>	8	1.0	64	10.0	.6
v <sub>3</sub>	4	•5	32	10.0	.6
V <sub>4</sub>	16	2.81	91	7.1	.6
V <sub>5</sub>	11.3	2.0	64	7.1	.6
v <sub>6</sub>	5.66	1.0	32	7.1	.6
v <sub>7</sub>	16	4.0	64	5.0	.6
v <sub>8</sub>	8	2.0	32	5.0	.6
v <sub>9</sub>	4	1.0	16	5.0	.6

TABLE II

LATERAL-FORCE DERIVATIVES OF VERTICAL TAILS ALONE AND

VERTICAL TAILS PLUS INTERFERENCE EFFECTS ON

TAILS - STRAIN-GAGE RESULTS

Vertical tail	~	(C <sub>w</sub> )	$(C_{Y_{\beta}})_{t+\Delta_{1}}$						
	α, deg	(CY <sub>β</sub> ) <sub>t</sub>	F <sub>1</sub> forward	F <sub>l</sub> rearward	F <sub>2</sub> forward	F <sub>2</sub> rearward	F3		
v <sub>l</sub>	0 10	0.0465	0.0577	0.0492	0.0514	0.0500 .0475	0.0527		
V <sub>2</sub>	0	.0326	.0384	.0333 .0344	.0386 .0364	.0350 .0342	.0368		
v <sub>3</sub>	0 10	.0212	.0263	.0223	.0251	.0238	.0258		
V <sub>1</sub> ,	0 10	.0567	.0693	.0617	.0666 .0645	.0639	.0673 .0644		
V <sub>5</sub>	0 10	.0477	.0622	.0532 .0544	.0586 .0560	.0595	.0592		
v <sub>6</sub>	0 10	.0351	.0463	.0387	.0464 .0427	.0411	.0445		
٧7	0 10	.0666	.0807	.0730	.0794 .0725	.0748 .0687	.0764		
V <sub>8</sub>	0 10	.0497	.0688	.0591	.0665		.0662		
V9	0 10	1	.0522	.0405	.0496		.0462		

TABLE III

STABILITY-DERIVATIVE DATA FOR COMPLETE MODEL AND

FUSELAGE ALONE - BALANCE-SYSTEM MEASUREMENTS

Coefficients based on  $S_W = 2.25 \text{ sq ft}$  and  $b_W = 3.0 \text{ ft}$ 

Configuration	$rac{s_{ extsf{t}}}{s_{ extsf{w}}}  c_{ extsf{Y}_{eta}}$		St Sw 1	Ow Cn <sub>β</sub>	St Sw bt Clβ		
	$\alpha = 0^{\circ}$	$\alpha = 10^{\circ}$	$\alpha = 0^{\circ}$	$\alpha = 10^{\circ}$	$\alpha = 0^{\circ}$	$\alpha = 10^{\circ}$	
		F	1, forwar	rd positi	on		
F <sub>1</sub> alone	-0.0035	-0.0030	-0.00171	-0.00179	0.00020	0.00014	
$F_1 + V_1$	0292	0281	.00873	.00976	00446	00260	
$F_1 + V_2$	0131	0130	.00223		00074		
F <sub>1</sub> + V <sub>3</sub>	0075	0073	.00001		.00013		
F <sub>1</sub> + V <sub>4</sub>	0248	0247	.00782	.00808	00464	00231	
F1 + V5	0179	0176	.00448	.00489	00169	00052	
F <sub>1</sub> + V <sub>6</sub>	0099	0093	.00110	.00132	00014	.00048	
F <sub>1</sub> + V <sub>7</sub>	0211	0201	.00646	.00626	00324	00170	
F <sub>1</sub> + V <sub>8</sub>	0120	0107	.00188	.00223	00120	00107	
F <sub>1</sub> + V <sub>9</sub>	0071	0069	.00005	.00003	.00019	.00040	
		F	<sub>l</sub> , rearwa	rd positi	ion		
F <sub>l</sub> alone	-0.0035	-0.0030	-0.00171	-0.00179	0.00020	0.00014	
$F_1 + V_1$	0248	0245	.01150	.01225	00393	00128	
F <sub>1</sub> + V <sub>2</sub>	0103	0100	.00309	.00321	00041	.00055	
$F_1 + V_3$	0054	0050	00021	00009	.00029	.00051	
F <sub>1</sub> + V <sub>4</sub>	0225	0216	.01010	.01067	00330	00120	
F <sub>1</sub> + V <sub>5</sub>	0150	0146	.00572	.00622	00126	.00010	
F <sub>1</sub> + V <sub>6</sub>	0076	0079	.00090		.00005	00056	
$F_1 + V_7$	0183	0178	.00794		00254	00085	
F <sub>1</sub> + V <sub>8</sub>	0093	0093	.00247		00026	.00046	
F <sub>1</sub> + V <sub>9</sub>	0058	0049	0		1	.00048	

TABLE III. - Continued

# STABILITY-DERIVATIVE DATA FOR COMPLETE MODEL AND

# FUSELAGE ALONE - BALANCE-SYSTEM MEASUREMENTS

[Coefficients based on  $S_W = 2.25 \text{ sq ft}$  and  $b_W = 3.0 \text{ ft}$ ]

Configuration	St Sw	$C_{Y_{\beta}}$	St Bw 1	Ot Cn <sub>β</sub>	St R	Ot Cla
	$\alpha = 0^{\circ}$	$\alpha = 10^{\circ}$	$\alpha = 0^{\circ}$	$\alpha = 10^{\circ}$	$\alpha = 0^{\circ}$	$\alpha = 10^{\circ}$
		F	2, forwa	rd positio	on	
F <sub>2</sub> alone	-0.0020	-0.0025	-0.00111	-0.00109	0.00013	0.00015
$F_2 + V_1$	0259	0249	.00587	.00644	00496	00336
$F_2 + V_2$	0122	0122	.00163	.00182	00082	00019
$F_2 + V_3$	0058	0063	.00003	.00003	.00005	.00029
$F_2 + V_4$	0242	0231	.00520	.00572	00441	00289
E . V	0173	0155	.00297	00330	00194	- 00098
$F_2 + V_5$	0173	0199	.00056		000194	
F <sub>2</sub> + V <sub>6</sub>	0195	0198	.00422		00346	
F <sub>2</sub> + V <sub>7</sub>	0197		.00122	1	00100	
F <sub>2</sub> + V <sub>8</sub>	0100		0		.00010	
$F_2 + V_9$	0000	00)9		.00012	**************************************	.0002)
		F <sub>2</sub>	, rearwa	rd position	on	
F2 alone	-0.0020	-0.0025	-0.00111	-0.00109		
$F_2 + V_1$	0243	0239	.00658	1	00445	
$F_2 + V_2$	0112	0112	.00164		00066	
$F_2 + V_3$	0060	1	.00002	1	.00011	
$F_2 + V_4$	0223	0217	.00584	.00642	00391	00242
$F_2 + V_5$	0150	0139	.00340	.00372	00165	00073
$F_2 + V_6$	0076	1	.00080	.00082	00012	.00020
F <sub>2</sub> + V <sub>7</sub>	0183	1	.00493	.00512	00314	00187
F <sub>2</sub> + V <sub>8</sub>	0097	1	.00161	.00163	00050	00004
$F_2 + V_9$	0059	1	0	0	.00010	.00030

TABLE III. - Concluded

# STABILITY-DERIVATIVE DATA FOR COMPLETE MODEL AND

FUSELAGE ALONE - BALANCE-SYSTEM MEASUREMENTS

Coefficients based on  $S_W = 2.25 \text{ sq ft}$  and  $b_W = 3.0 \text{ ft}$ 

Configuration	$\frac{s_t}{s_w}$ $c_{Y_{\beta}}$		St Sw	bt Cnβ	St Sw ClB		
	The second secon	$\alpha = 10^{\circ}$	$\alpha = 0^{\circ}$	$\alpha = 10^{\circ}$	$\alpha = 0^{\circ}$	$\alpha = 10^{\circ}$	
			F	3			
F <sub>3</sub> alone	-0.0019	-0.0013	-0.00080	-0.00080	0.00010	0.00022	
$F_3 + V_1$	0259	0239	.00424	.00473	00457	00358	
$F_3 + V_2$	0126	0120	.00100	.00136	00082	00042	
F3 + V3	0060	0062	0	0	0	.00016	
F <sub>3</sub> + V <sub>4</sub>	0239	0223	.00375	.00426	00421	00311	
F3 + V5	0166	0153	.00220	.00244	00182	00122	
F <sub>3</sub> + V <sub>6</sub>	0079	0083	.00051	.00059	00032	0	
F <sub>3</sub> + V <sub>7</sub>	0198	0181	.00319	.00338	00347	00239	
F <sub>3</sub> + V <sub>8</sub>	0106	0097	.00093	.00111	00066	00032	
F <sub>3</sub> + V <sub>9</sub>	0055	0050	0	0	0	.00015	

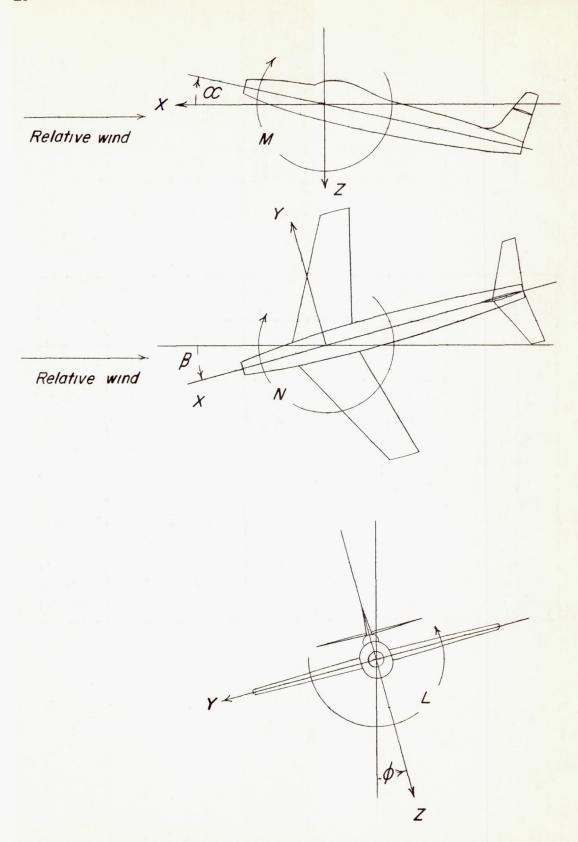
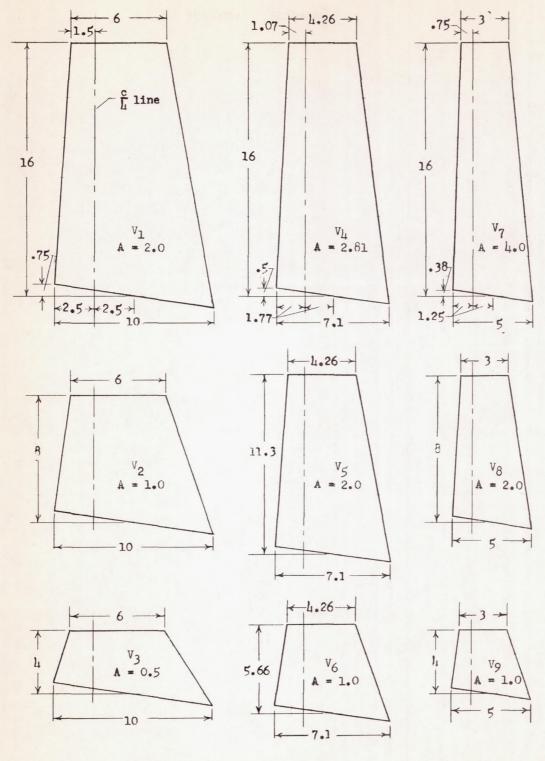


Figure 1.- The stability system of axes. Arrows indicate positive directions of forces, moments, and angles.



(a) Vertical tails.

Figure 2.- Sketches of the models used in this investigation. (All dimensions are in inches.)

			F1 Forward	F <sub>1</sub> Rearward	F <sub>2</sub>	F <sub>2</sub> Rearward	F3
		l <sub>t</sub>	15.38	22.5	9.75	12.56	7.5
		D	4.5	2.5	4.5	3.38	4.5
	60	<u> </u>	Tail C 1	DDA	<del>\</del>	6*	
	F <sub>1</sub>		4				
Center of gravity	140 It					6	
	30					6	
	F <sub>3</sub>						

(b) Fuselages.

Figure 2.- Concluded.

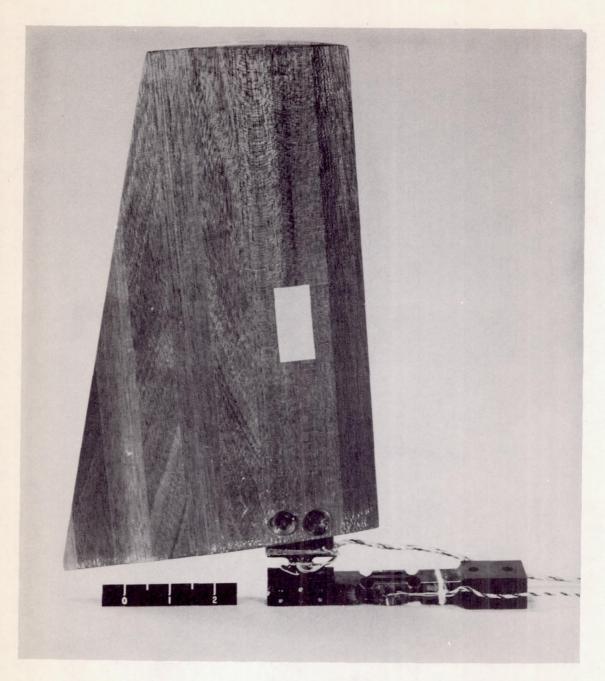


Figure 3.- A vertical tail attached to a strain gage. L-76419

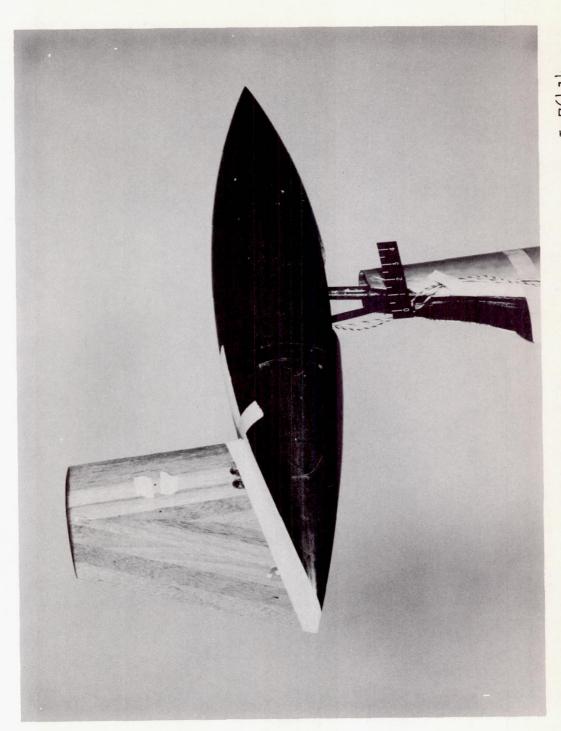


Figure 4.- A complete model mounted on the support strut. L-76414

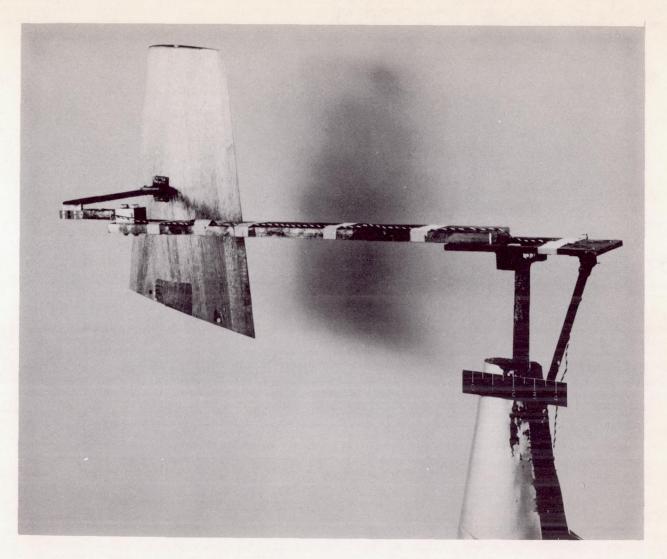


Figure 5.- Vertical-tail mounting for determining isolated-vertical-tail L-76416 results.

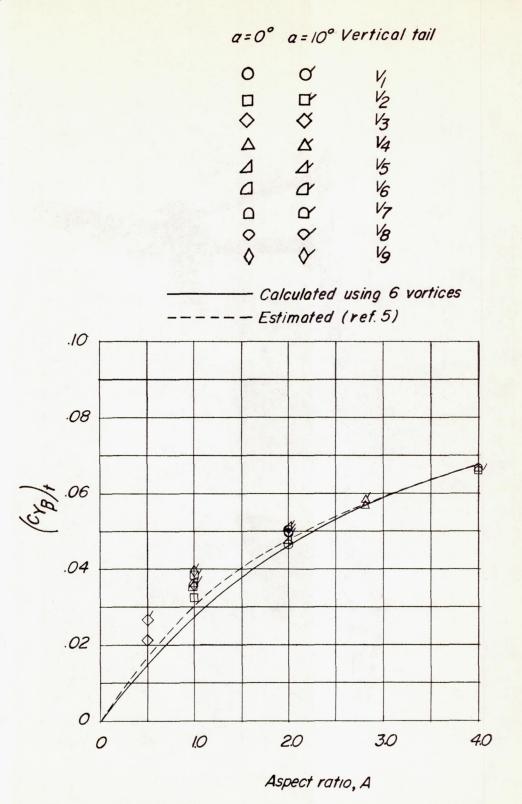


Figure 6.- Measured and estimated values of lateral-force derivatives for isolated vertical tails.

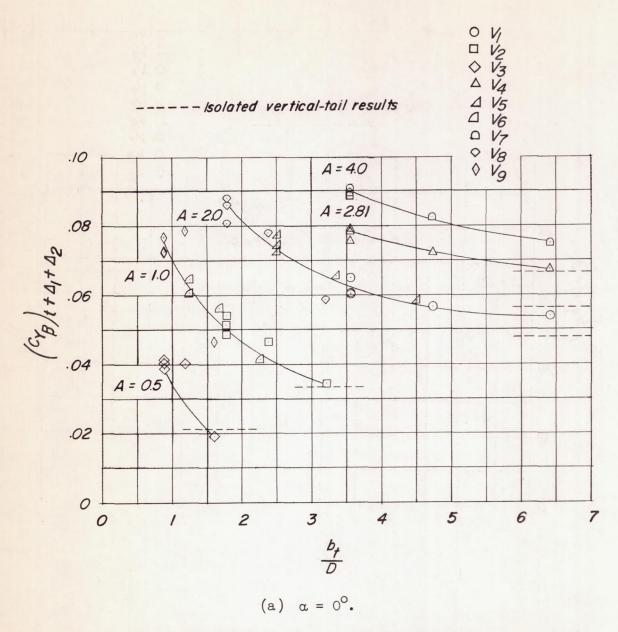


Figure 7. - Lateral-force derivatives for vertical tails plus mutual interference effects on the tail-fuselage combination.

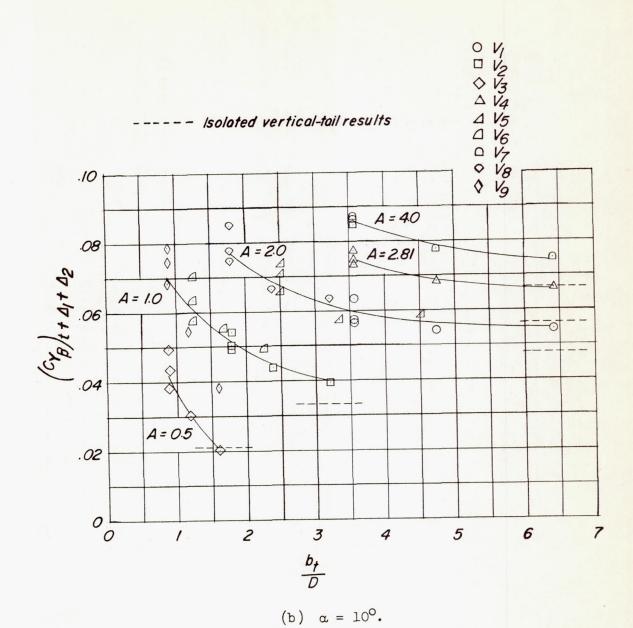


Figure 7.- Concluded.

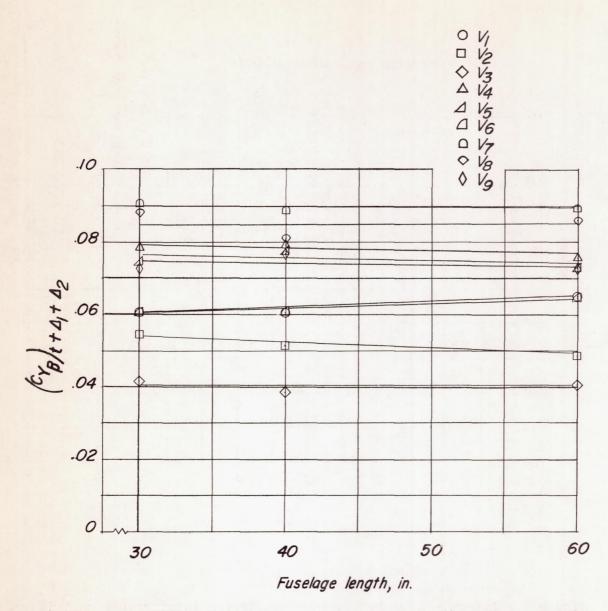


Figure 8. - Variation of lateral-force derivatives of vertical tails plus mutual interference effects with fuselage length.  $\alpha = 0^{\circ}$ .

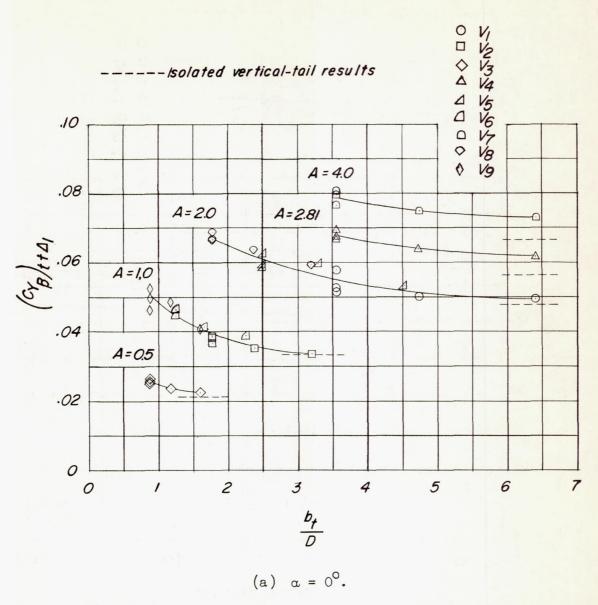


Figure 9.- Lateral-force derivative results for interference on tails of vertical tails plus fuselage.

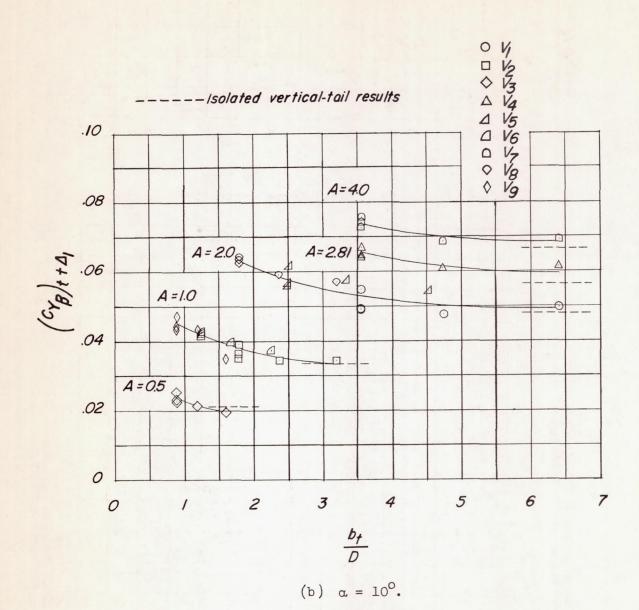
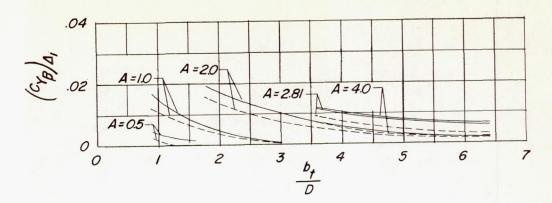
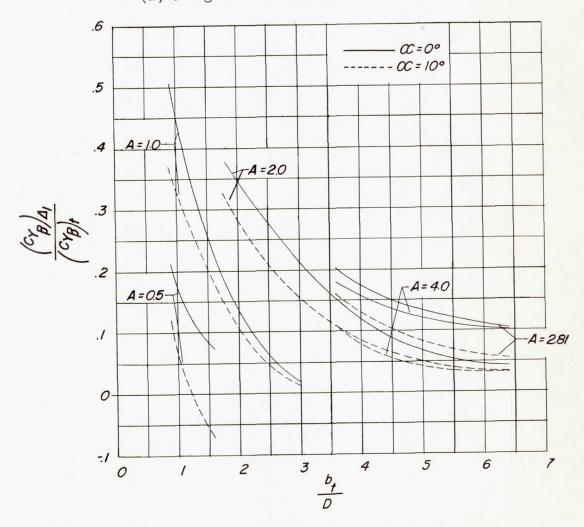


Figure 9. - Concluded.

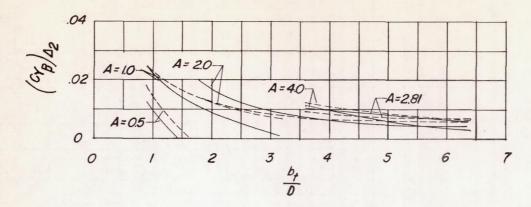


(a) Change in lateral-force derivative.

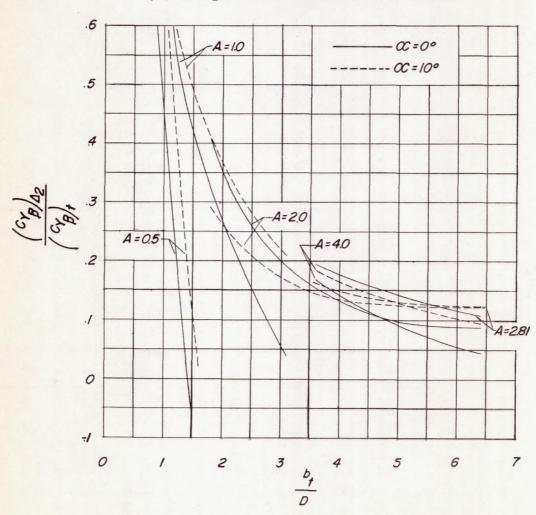


(b) Ratio of lateral-force-derivative increment to isolated-vertical-tail values.

Figure 10. - Interference effect of fuselage on vertical tail.



(a) Change in lateral-force derivative.



(b) Ratio of lateral-force-derivative increment to isolated-vertical-tail values.

Figure 11.- Interference effect of vertical tail on fuselage.

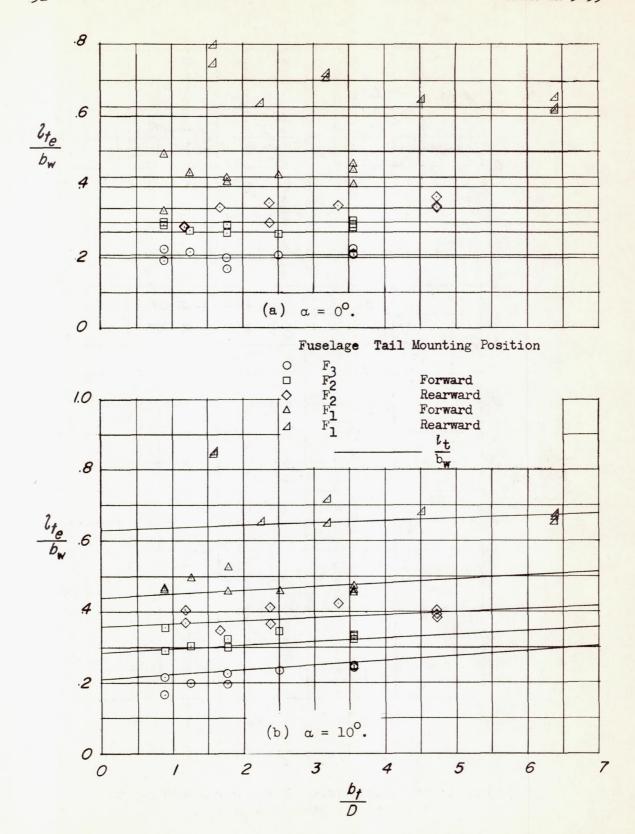


Figure 12. - Effective tail lengths compared with geometric tail lengths.

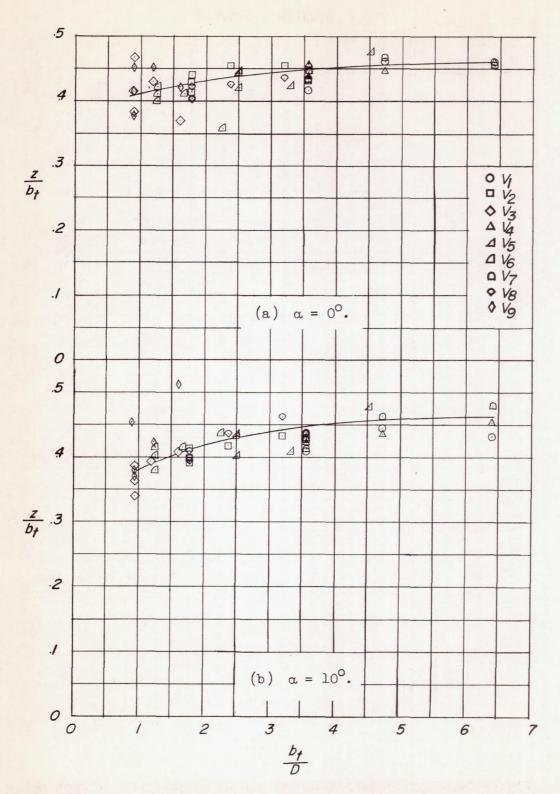


Figure 13.- Vertical location of center of pressure of loading on vertical tail  $({}^{C}Y_{\beta})_{t+\Delta_{l}}$ .

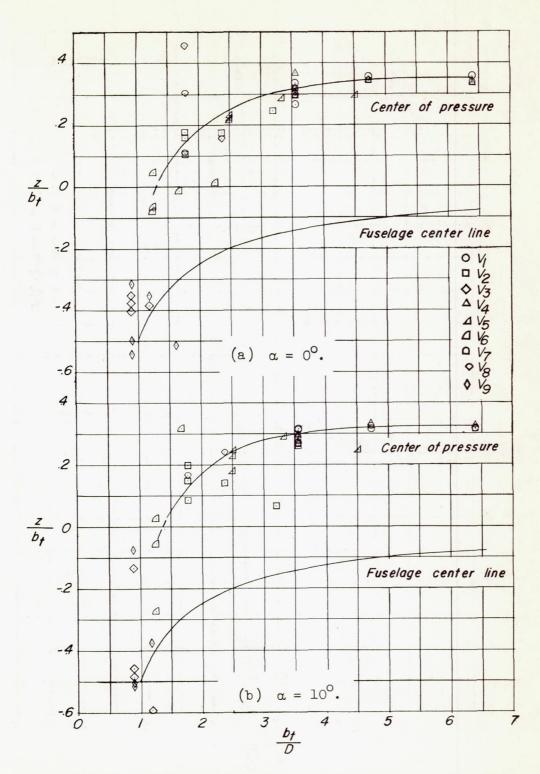


Figure 14.- Vertical location of center of pressure of combined loading  $({}^{\rm C}{}_{\rm Y}{}_{\beta})_{t+\Delta_1+\Delta_2}$ .

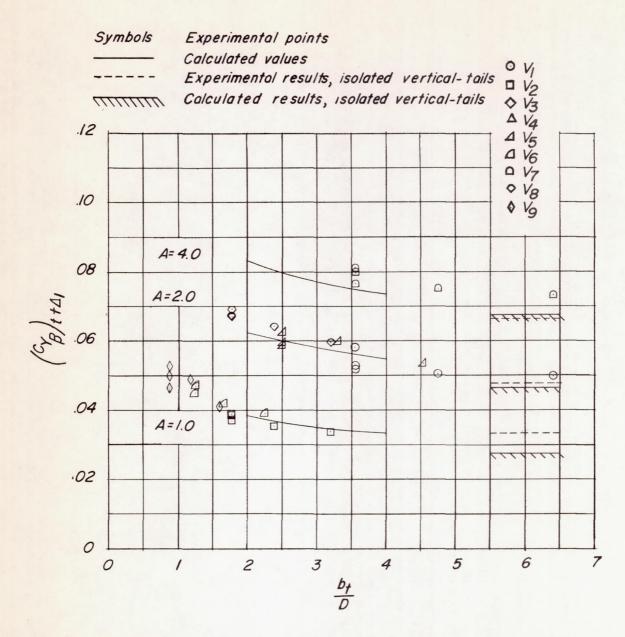


Figure 15.- Results of lateral-force-derivative calculations compared with experimental results.  $\alpha = 0^{\circ}$ .